On Proton Conductivity in Porous and Dense Yttria Stabilized Zirconia at Low Temperature

Barbara Scherrer, Meike V.F. Schlupp, Dieter Stender, Julia Martynczuk, Jan G. Grolig, Huan Ma, Peter Kocher, Thomas Lippert, Michel Prestat, and Ludwig J. Gauckler*

The electrical conductivity of dense and nanoporous zirconia-based thin films is compared to results obtained on bulk yttria stabilized zirconia (YSZ) ceramics. Different thin film preparation methods are used in order to vary grain size, grain shape, and porosity of the thin films. In porous films, a rather high conductivity is found at room temperature which decreases with increasing temperature to 120 °C. This conductivity is attributed to proton conduction along physisorbed water (Grotthuss mechanism) at the inner surfaces. It is highly dependent on the humidity of the surrounding atmosphere. At temperatures above 120 °C, the conductivity is thermally activated with activation energies between 0.4 and 1.1 eV. In this temperature regime the conduction is due to oxygen ions as well as protons. Proton conduction is caused by hydroxyl groups at the inner surface of the porous films. The effect vanishes above 400 °C, and pure oxygen ion conductivity with an activation energy of 0.9 to 1.3 eV prevails. The same behavior can also be observed in nanoporous bulk ceramic YSZ. In contrast to the nanoporous YSZ, fully dense nanocrystalline thin films only show oxygen ion conductivity, even down to 70 °C with an expected activation energy of 1.0 ± 0.1 eV. No proton conductivity through grain boundaries could be detected in these nanocrystalline, but dense thin films.

1. Introduction

Yttria-stabilized-zirconia (YSZ) thin films are potential electrolytes for sensors or micro-solid oxide fuel cells and show pure oxygen ion conductivity when measured at higher temperatures.[1] Proton conductivity in YSZ single crystals at high temperatures has been reported by Wagner[2a] and later by Y. Nigara et al.[2b] Wagner extrapolated the water solubility in YSZ at 1000 °C and 1 atm H_2O to be 1×10^{-4} mol H_2O per mol YSZ. With permeation measurements of H_2 through a polycrystalline YSZ tube, he calculated a proton conductivity of $\sigma_{Hi} = 1.3 \times 10^{-3}$ S m^{-1} at 1000 °C and concluded that the proton conductivity is negligible compared to the oxygen ion conductivity. Similar results were also obtained for $(CeO_2)_{0.9}(GdO_{1.5})_{0.1}$ by the Mizusaki group.[3]

Recent studies have shown the electrical conductivity of nanocrystalline zirconia- and ceria-based oxides to increase with decreasing temperature below 150 °C.[4–6,7–11] This effect was attributed to the migration of protons in the nanocrystalline material; as in a dry atmosphere, no, or a very low proton conductivity was found for microcrystalline and nanocrystalline zirconia and ceria-based ceramics.[4,5] It is also known from resistivity measurements of metal oxide gas sensors that the signal is highly dependent on humidity. One example of humidity sensors was reported by Wang et al., who observed a drastic decrease of the resistivity with increasing humidity.[12] However, it is under debate whether the protons are conducted along the YSZ surface or through its grain boundaries. For proton conductivity in YSZ, it has been reported that increasing proton conductivity occurs with decreasing grain size, which leads to the conclusion that the grain boundaries conduct the protons.[5–7] This is supported by the findings of Kim et al. who presented an open circuit voltage across an electrochemical cell with such electrolytes of 110 mV at 25 °C in a water gradient of distilled water and humid air.[13] However, Shirpour et al. raised doubts that grain boundaries in YSZ conduct protons as their mobility at the grain boundary would be too low for the measured conductivity.[4] This is supported by a very recent study of Tandé et al.[9] Raz et al. investigated the conductivity of YSZ powder compacts at low temperatures and the effect of humidity on conduction.[10,11] The resistance decreased drastically below 100 °C in humid air and they attributed this conductivity to protons along physisorbed and chemisorbed water on the YSZ powder surface.

In a recent study, we have demonstrated that pores of less than 10 nm in YSZ thin films still form a continuous

B. Scherrer, M. V. F. Schlupp, Dr. J. Martynczuk, J. G. Grolig,H. Ma, P. Kocher, Dr. M. Prestat, Prof. Dr. L. J. Gauckler
Nonmetallic Inorganic Materials
ETH Zurich, Wolfgang-Pauli-Str.10,
CH-8093 Zurich, Switzerland
E-mail: barbara.scherrer@mat.ethz.ch
D. Stender, Dr. T. Lippert
General Energy Research Department
Paul Scherrer Institut
CH-5232 Villigen-PSI, Switzerland
Prof. Dr. L. J. Gauckler
International Institute for Carbon Neutral Energy Research (WPI-I2CNER), Kyushu University
744 Moto-oka, Nishi-ku, Fukuoka 819-0395, Japan

DOI: 10.1002/adfm.201202020

percolating network throughout the sample.[14] Therefore, we investigated the conductivity in YSZ thin films in order to elucidate whether the proton conductivity is due to adsorbed water at the inner surface of porous specimens or whether it is related to H^+-migration through grain boundaries of nanocrystalline YSZ.

The aim of this study is to report the microstructures and conductivity of nanocrystalline YSZ thin films from room temperature to 400 °C. YSZ thin films were deposited by different methods in order to vary their porosity, grain size, and shape. The electrical conductivity was measured by impedance spectroscopy in a cross-plane configuration that allows reliable measurements even down to room temperature.

2. Results

2.1. Influence of the Preparation Techniques on YSZ Microstructures

The microstructures of the YSZ thin films and bulk specimens deposited by different techniques are described, as follows, and their characteristic microstructural features are summarized in **Table 1**.

2.1.1. Spray Pyrolysis (SP) Thin Films

The YSZ thin films deposited by SP are predominately amorphous with a few embedded crystalline nuclei of 3-nm diameter.[15] During heating, the material starts to crystallize and to develop grain boundaries. The films annealed at 600 °C for 0 h are ≈30% crystalline according to DSC measurements with a grain size of 5 nm determined by XRD and TEM.[15] The YSZ reaches full crystallinity either by a further increase in temperature (T ≥ 900 °C) or by an isothermal dwell above 600 °C ($t \geq 17$ h). The crystals grew to 9 and 13 nm after an isothermal dwell for 20 h at 600 and 800 °C, respectively. All heat-treated thin films are nanoporous with a pore size similar to the grain size.[14] As an example, an STEM micrograph of a SP thin film annealed at 600 °C for 20 h is shown in **Figure 1**a, where grains (bright) and pores (dark) are visible. According to fluctuation in Z-contrast observed in the STEM micrographs (not shown here; see ref. [14]), the as-deposited thin films are most likely porous, although some of the contrast might also be due to residual organic material. For thin films annealed at 800 °C for 20 h a porosity of about 43 vol% was estimated by FIB nanotomography.[14] In summary, the SP films show randomly oriented nanocrystalline microstructures with different grain sizes as shown in Table 1, depending on the temperature and annealing duration. More details on the microstructural changes during heat treatments and the porosity can be found in the literature.[14,15]

2.1.2 AA-CVD Thin Films

Thin films prepared by AA-CVD at 450 °C and annealed at 600 °C exhibit randomly oriented nanocrystalline microstructures featuring nanoporosity (Figure 1b). These microstructures are very similar to those of the SP films (compare Figure 1a with Figure 1b). Both deposition techniques (SP and AA-CVD) are nonvacuum techniques based on organometallic precursors. Nevertheless, the deposition mechanism is totally different. Further information on the porosity and the deposition mechanism are reported elsewhere.[14,16,17] At higher substrate temperatures (600 °C), thin films with columnar grains are deposited, which feature only a few pores of about 5 nm embedded in the grains (Figure 1c). More details of the microstructure of AA-CVD films are given elsewhere.[16,17]

Table 1 Microstructural features of YSZ thin films and bulk materials with respect to the preparation techniques, preparation parameters and annealing conditions.[15,18,20]

	Yttria content	Preparation technique	Preparation conditions[a)]	Annealing conditions	Microstructure	Grain size [nm]	Crystallinity [%]
Thin films	8YSZ	SP	370 °C	As-deposited	porous, equiaxed grains	3	0
		SP	370 °C	600 °C, 0 h	porous, equiaxed grains	5	27
		SP	370 °C	600 °C, 20 h	porous, equiaxed grains	9	100
		SP	370 °C	800 °C, 20 h	porous, equiaxed grains	13	100
		AA-CVD	450 °C	600 °C, 20 h	porous, equiaxed grains	8	100
		AA-CVD	600 °C	600 °C, 20 h	dense, columnar grains	10 to 20[b)]	100
		PLD	700 °C, 2.7 Pa	600 °C, 1 h	dense, columnar grains	20[b)]	100
	3YSZ	PLD	450 °C, 7 Pa	600 °C, 1 h	porous, columnar grains	20[b)]	100
		PLD	450 °C, 1 Pa	600 °C, 1 h	dense, columnar grains	20[b)]	100
bulk materials	8YSZ tape	Sintering of powder	1350 °C	n.a.	dense, equiaxed grains	6×10^3	100
	3YSZ bulk	Sintering of powder	850 °C	n.a.	50 vol% porous, equiaxed grains	40	100

[a)]substrate temperature and oxygen partial pressure or sintering temperature; [b)]column width.

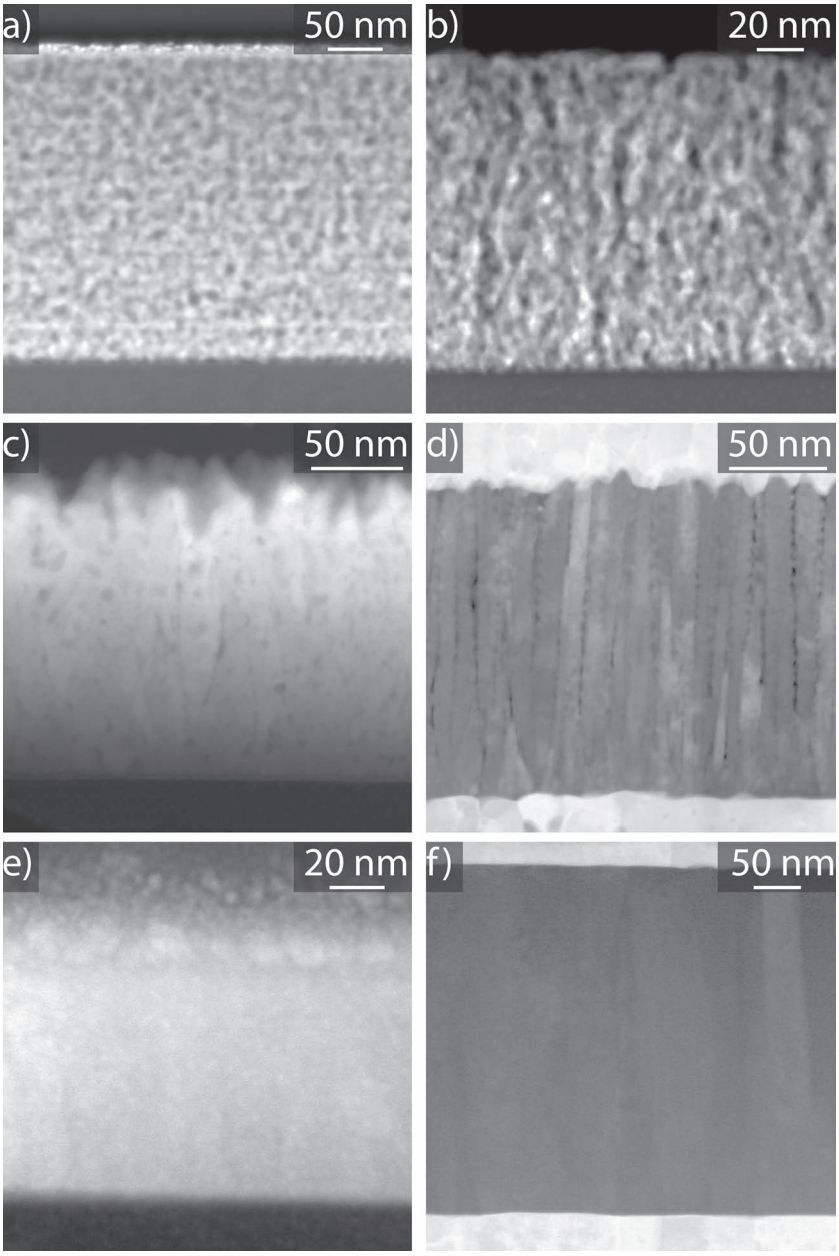

Figure 1. HAADF STEM micrographs of YSZ thin films deposited by different methods. a) 8YSZ SP (T_{dep} = 370 °C; T_{pa} = 600 °C, 20 h), b) 8YSZ AA-CVD (T_{dep} = 450 °C, T_{pa} = 600 °C, 20 h), c) 8YSZ AA-CVD (T_{dep} = 600 °C, T_{pa} = 600 °C for 20 h), d) 3YSZ PLD (T_{dep} = 450 °C, p_{O2} = 7 Pa, T_{pa} = 600 °C, 1 h) with top and bottom electrode, e) 3YSZ PLD (T_{dep} = 450 °C, p_{O2} = 1 Pa, T_{pa} = 600 °C, 1 h), and f) 8YSZ PLD (T_{dep} = 700 °C, p_{O2} = 2.7 Pa, T_{pa} = 600 °C, 20 h) with top and bottom electrodes.

2.1.3. PLD Thin Films

Microstructures of YSZ thin films prepared by PLD are shown in Figure 1d–f. For the PLD thin films shown in Figures 1d–f, specimens with Pt electrodes were analyzed to exclude the possible influence of the Pt electrodes on the YSZ microstructure. The grains are columnar with a width of 20 nm and have a (101) and (002) texture for 3YSZ, and a (111) texture for 8YSZ.[18] All PLD films are free of organic residues as they result from ablation of a ceramic target in vacuum. For depositions at an oxygen partial pressure of 7 Pa in the PLD chamber, channel-like pores are present between the columnar grains (Figure 1d). However, fully dense films can be obtained by lowering the deposition pressures (≤ 2.7 Pa) as shown in Figure 1e (3YSZ) and Figure 1f (8YSZ). This is in good agreement with our earlier findings for YSZ and $Ce_{08}Gd_{0.2}O_{1.98}$ thin films prepared by PLD.[19]

2.1.4. Sintered Bulk Materials

Figure 2 shows the microstructures of sintered microcrystalline 8YSZ tape and porous nanocrystalline 3YSZ bulk material. The average grain size for the dense tape is 6 µm (Figure 2a). The porous nanocrystalline 3YSZ bulk material has a porosity of 50 vol% with an average grain size of 40 nm (Figure 2b).

2.2. Electrical Conductivity of YSZ Thin Films

A typical impedance spectrum at 50 °C of a thin film deposited by spray pyrolysis and annealed at 600 °C for 0 h is shown in **Figure 3**. From the total resistance of the electrolyte the total electrical conductivity was evaluated. All measurements were conducted on an open setup under ambient conditions.

The electrical conductivities of YSZ thin films deposited by different techniques and annealed under different conditions are shown in **Figure 4**a,b. At temperatures above 400 °C (regime A) the total electrical conductivity of all films is dominated by pure oxygen ion conduction with an activation energy of 0.9–1.3 eV as expected. This regime is discussed in more detail in a separate publication.[20]

As shown in regime B of Figure 4a, the conductivity of porous YSZ thin films spreads over almost two orders of magnitude below 400 °C for different samples. Even for different measurements carried out at different times on the very same sample, a variation over two orders of magnitude was measured. This leads to the conclusion that the humidity (in the laboratory atmosphere) influences the electrical conductivity to a greater extent than the amount of porosity or other microstructural properties. The corresponding activation energies range from 0.4 to 1.1 eV. At around 120 °C, all porous films show a minimum in conductivity. Below 120 °C (regime C in Figure 4a), the conductivity increases with decreasing temperature. Additionally, the sensitivity of the electrical conductivity was estimated by directing a humidified air flow to the specimen surface. The conductivity increases during humidification, especially in regime C. This

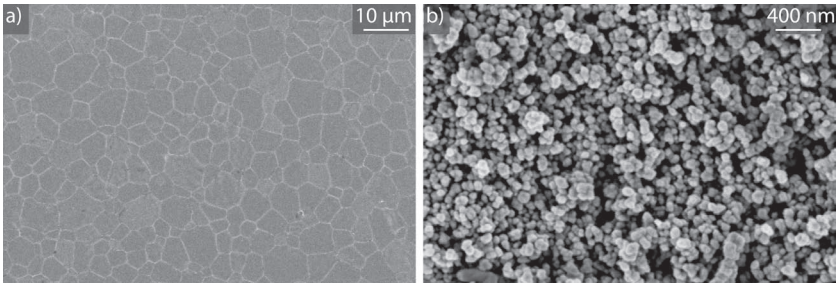

Figure 2. SEM micrographs of a) dense microcyrstalline 8YSZ tape and b) 50 vol% porous nanocrytsalline 3YSZ.

result is not shown here, as the measurements were not conducted in thermodynamic equilibrium. The absolute value of the conductivity is not correlated with one of the microstructural properties such as the grain size or crystallinity.

The conductivity of dense but nanocrystalline YSZ thin films is shown in Figure 4b. The dense thin films (grain size: 10 to 20 nm) show thermally activated conductivities from high (450 °C) to low (100 °C) temperatures only. Below 100 °C, the resistance exceeded the measurable range of our impedance device. Activation energies of 1.1 and 1.0 eV were found for 8YSZ and 3YSZ thin films, respectively.

2.3. Electrical Conductivity of Porous and Dense Bulk YSZ

The electrical properties of dense and porous YSZ bulk specimens with different microstructures were measured in dry and humid air. **Figure 5**a shows the total electrical conductivity of the dense microcrystalline YSZ tape measured in direct current mode. The steps in the conductivity data are artifacts related to the direct current equipment. The electrical conductivity follows an Arrhenius-type behavior and is independent on the humidity down to 100 °C with activation energies of 0.8 ± 0.1 eV. In Figure 5b, the electrical conductivity of the porous, nanocrystalline YSZ bulk specimen is shown. The measurements were carried out in direct and alternating current modes to exclude a systematic error due to the measurement mode. In dry air and direct current mode, it was possible to record the data down to 150 °C. The data follow an Arrhenius behavior with an activation energy of 1.0 eV. In the alternating current mode spectra could be obtained down to room temperature. Below 120 °C, these data become independent of temperature. However, at these low temperatures water from the humid laboratory air is likely to diffuse into the open furnace used for the alternating current measurements and may have condensed on and inside the porous specimen. In humid air, the electrical conductivity of the porous samples resemble the behavior of the porous thin films. From high temperatures down to ≈400 °C it follows an Arrhenius behavior with an activation energy of 1.0 eV. Below 400 °C, the conductivity is enhanced compared to the data obtained in dry air (regime B). The conductivity changes gradually resulting in a continuous decrease of the thermal dependence and thereby leading a decreasing activation energy. Additionally, the conductivity increases with decreasing temperature from below 120 °C to room temperature, regardless of the measurement mode (direct and alternating current).

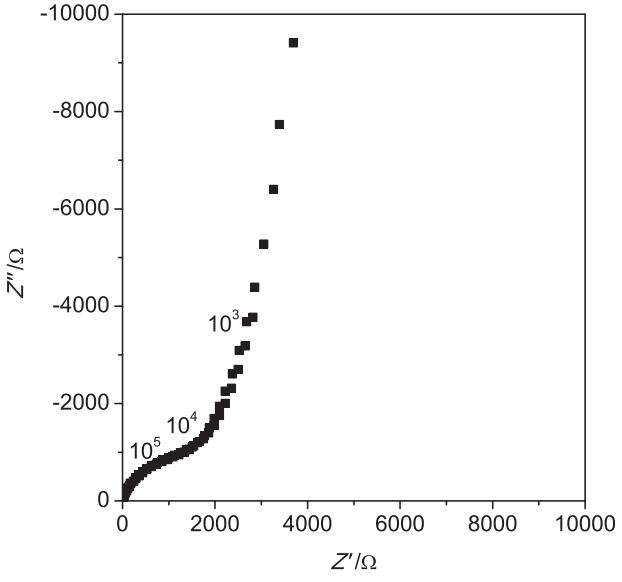

Figure 3. Typical impedance spectrum at 50 °C of an YSZ thin film deposited by spray pyrolysis and annealed at 600 °C for 0 h.

3. Discussion

The electrical conductivity data of the porous materials presented in this paper can be divided into three temperature regimes: (i) temperatures higher than 400 °C (A), (ii) temperatures between 120 and 400 °C (B) and (iii) temperatures lower than 120 °C (C). In the high temperature regime (A, T > 400 °C), the electrical conductivity is only dependent on the microstructure and dopant, and not on the humidity, which is in accordance to published data.[21] In this temperature range, the conductivity is exclusively caused by the migration of oxygen ions. Further details separating grain and grain boundary conductivity are discussed elsewhere.[20]

Between 400 °C and room temperature, the conductivity of the porous materials is highly sensitive to moisture. The lack of reproducibility from measurement to measurement obtained for the porous thin films is due to an uncontrollable humidity in the open measurement setup. If the humidity is controlled, as it was done for the direct current measurements of the bulk specimens (closed furnace), reproducible values are obtained (Figure 5). In the following section, the two temperature regimes (B and C) of the electrical conductivity are discussed and conduction mechanisms are proposed.

3.1. Temperature Regime between 120 and 400 °C

In the temperature regime B (from 400 down to 120 °C), the porous specimens show a drastically increased conductivity in

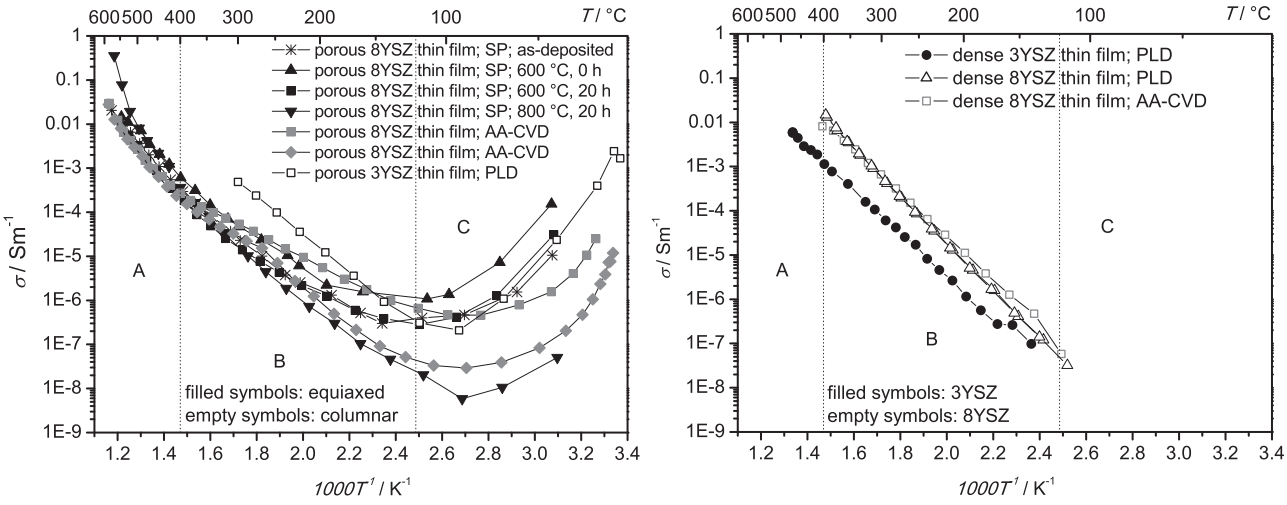

Figure 4. Total electrical conductivity of YSZ thin films measured in laboratory atmosphere. The data was acquired during cooling, except for the as-deposited SP thin film (heating curve). a) Porous thin films prepared by SP (deposited at 370 °C, as-deposited: ∗; post-annealed at 600 °C for 0 h: ▲; 600 °C for 20 h: ■; 800 °C for 20 h: ▼), AA-CVD: ■ and ◆ (deposited at 450 °C, post-annealed at 600 °C for 20 h) and PLD: □ (deposited at 450 °C, p_{O2} = 7 Pa (3YSZ) and post-annealed at 600 °C for 0 h). b) Dense thin films prepared by AA-CVD: □ (deposited at 600 °C and post-annealed at 600 °C for 20 h); and PLD: ● (deposited at 450 °C, p_{O2} = 1 Pa (3YSZ) and post-annealed at 600 °C for 0 h) and △ (deposited at 700 °C, p_{O2} = 2.7 Pa (8YSZ) and post-annealed at 600 °C for 20 h).

humid air compared to the dense specimens or porous specimens measured in dry air. This spread is observed for thin films as well as bulk samples. At temperatures of 400 °C and lower, water starts to adsorb chemically on the oxide surfaces, most likely at the vacancy sites and dissociation then results in hydroxyl groups.[11,22,23] These hydroxyl groups start to desorb at temperatures above 250 °C, but some persist even after heat treatments at 500 °C.[23–25] The electrical conductivity of zirconia hydrate and zirconia with chemisorbed water shows an activation energy of about 0.3 eV.[11,26] The activation energies for the porous specimens in our study are somewhat higher with 0.4 to 1.1 eV. This suggests that besides the oxygen ion conductivity manly proton conduction contributes to the measured total conductivity. The degree of the hydroxylation is correlated with the humidity and is reflected in the absolute conductivity value and in the activation energy. It can be concluded that the hydroxyl groups which are present at the inner surface of the porous YSZ are the reason for the enhanced conductivity and the lower activation energy observed in a humid atmosphere. No evidence of proton conduction through grain boundaries was obtained as no enhanced conductivity was found for dense but nanocrystalline specimens (grain size: 10–20 nm).

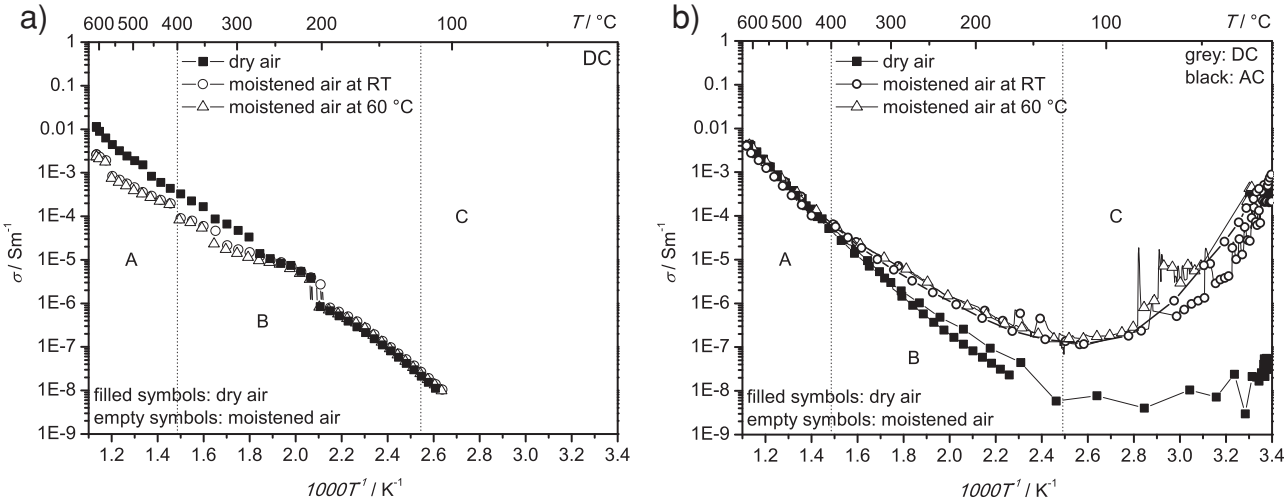

Figure 5. Electrical conductivity of a) dense 8YSZ tape with ≈6 µm grain size and b) porous 3YSZ pellet with ≈40 nm grain size. The specimens were measured in dry and moistened air. Data measured during cooling are shown.

3.2. Temperature Regime below 120 °C

In the low-temperature regime (regime C, T < 120 °C), the electrical conductivity increases with decreasing temperature, but again only for porous specimens. Below 120 °C, physisorbed water is present at the YSZ surface of the percolating nanoporous network in addition to the chemisorbed water. The physisorbed water partially dissociates like normal water and forms OH^- and H_3O^+ ions. The proton of a H_3O^+ ion is transferred from one water molecule to a lone pair of the neighboring water molecule. This transport mechanism is known as the Grotthuss mechanism and is described elsewhere in detail.[27] This proton conductivity is not thermally activated but varies at least over one order of magnitude depending on the relative humidity at a fixed temperature.[24,26,28] When changing temperature only, the relative humidity increases by a factor of 25 with decreasing temperature from 100 °C to room temperature and as a consequence, the absorbed water increases.[29] This results in an exponential increase of the physisorbed water molecules on the zirconia surface with decreasing temperature at fixed absolute water content in the atmosphere.[30] The enhanced coverage of physisorbed water at the surface of the YSZ results in an increased conduction path width for the protons, which are the mobile species. The larger conduction path width overcompensates the only slightly thermally-activated mobility of the protons. This conduction path over the pore surface explains the strong dependence on the water partial pressure as well as the independence of the dopant concentration reported here and in literature.[5,7] The surface of the pores (i.e., the porosity and tortuosity) is more important than the grain size for this conduction mechanism. We can thus conclude that the protonic conductivity at temperatures below 120 °C in the YSZ is due to proton migration via the internal surface, whereas the lattice and grain boundary conductivity is too low at these temperatures. This is supported by results of dense nanocrystalline and dense microcrystalline YSZ specimens which showed no conductivity in humid air at room temperature (Figure 4b and Figure 5a). The few measurement points at room temperature are thought to be caused by protons which are conducted via the external surface[9–11] and not through the bulk or grain boundaries as suggested in the literature.[5–8]

4. Conclusions

The cross-plane conductivity of YSZ thin films and bulk specimens, both dense and nanoporous, was measured down to room temperature. Three different conduction mechanisms are present in porous YSZ depending on the temperature regime. Above 400 °C, the electrical conductivity is exclusively due to the migration of oxygen ions. Between 400 and 120 °C, the enhanced conductivity in porous materials is due to transport of protons via chemisorbed water at the inner surface (pore walls) in addition to oxygen ion conductivity. The protons are formed by the dissociation of water to hydroxyl groups. Below 120 °C down to room temperature, conductivity in porous YSZ increases with decreasing temperature. This conductivity is due to the migration of protons within the physisorbed water over the inner surface of YSZ which increases as the thickness of the adsorbed water layer increases with decreasing temperature. In dense nanocrystalline YSZ, only oxygen ion conduction prevails down to 70 °C, which leads to the conclusion that grain boundaries are not permeable to protons.

5. Experimental Section

Thin Film Deposition: 8 mol% yttria-stabilized-zirconia (8YSZ) thin films were deposited by wet spray pyrolysis (SP); details on this method are found in reference [31]. The precursor solution was pumped to a spray gun (Compact 2000KM, Bölhoff Verfahrenstechnik, Germany) where it was atomized with 1 bar air pressure and sprayed on substrates heated to 370 ± 5 °C. The precursor solution consisted of zirconium 2,4-pentane dionate (ABCR, 95% purity) and yttrium chloride hydrate (Alfa Aesar, 99.9% purity) dissolved in 80 vol% tetraethylene glycol (TEG, Aldrich, 99%), 10 vol% polyethylene glycol 600 (PEG 600, Fluka) and 10 vol% ethanol (Fluka, 99.9%). The total salt concentration was 0.05 mol L^{-1}, corresponding to 0.0426 mol L^{-1} zirconium 2,4-pentane dionate and 0.0074 mol L^{-1} yttrium chloride hydrate. A molar ratio of Zr: Y = 85.2: 14.8 was chosen to obtain a 8 mol% yttria-stabilized zirconia film composition.[32] The liquid flow rate was 5 mL h^{-1} and two spray cycles of 20 min with intermediate cooling to room temperature were conducted for each film. The working distance between the spray nozzle and the hot plate was kept at 39 cm during all experiments.

For 8YSZ thin film deposition by aerosol-assisted chemical-vapor-deposition (AA-CVD), precursor solutions consisting of zirconium 2,4-pentane dionate (95% purity, ABCR) and yttrium 2,4-pentane dionate (99.9% purity, Alfa Aesar) in pure ethanol (>99.8% purity, A15 Alcosuisse) were nebulized in a custom-made spray setup.[16] The nebula was transported to a heated substrate (450 or 600 °C) using synthetic air (600 °C) or N_2 (99.995% purity, Pangas; 450 °C) at a flow rate of 4 L min^{-1} as carrier gas. The total metal concentrations were 0.025 mol L^{-1} (450 °C) or 0.005 mol L^{-1} (600 °C). The Zr: Y ratio of the solutions was set to 80: 20 to obtain Zr: Y ratios of 84: 16 in the thin films.[16]

Pulsed laser deposition (PLD) was used to deposit fully crystalline 3 mol% yttria-stabilized-zirconia (3YSZ) thin films at a temperature of 450 °C. The cylindrical target was fabricated from 3YSZ powder (Tosoh Corp., Japan) by uniaxial pressing at 4×10^8 Pa and subsequent sintering for 4 h at 1400 °C. The ablation was done with a KrF excimer laser at a wavelength of 248 nm (Lambda Physik, Germany). To reach a fluence of 1.2 J cm^{-2} the laser beam was reduced by a lens to a rectangular area of 2.2 mm^2. The substrates were placed on a rotating sample holder at a distance of 4 cm from the revolving target. A total of 24 000 pulses at a repetition rate of 5 Hz were used. The depositions were performed in an oxygen atmosphere at a pressures of 1.0 and 7.0 Pa. In the case of PLD 8YSZ thin films, the pill target was sintered from 8YSZ powder (Tosoh Corp., Japan) for 4 h at 1400 °C. The ablation was performed in a PLD workstation (Surface, Germany) with a KrF Excimer Laser (25 000 pulses at 10 Hz). The fluence was 2.9 J cm^{-2} and the distance from the target to the substrate 8.5 cm. Depositions were conducted at 700 °C at an oxygen chamber pressure of 2.66 Pa.

After deposition, the YSZ thin films were subsequently annealed at temperatures between 600 and 800 °C in ambient air. The thicknesses of the thin films were determined from cross-sectional SEM micrographs.

YSZ Bulk Samples: Porous 3YSZ samples were prepared by isostatic pressing (300 MPa) of 3YSZ powder (TZ-3YB, Tosoh Corp., Japan). The pressed cylinders were sintered at a rate of 1 °C min^{-1} up to 850 °C with a dwell time of 120 min. This resulted in a 50 vol% porous 3YSZ material from which a 1-mm-thin sample with ø = 2.5 cm was cut. The mean pore diameter after sintering was 25 nm measured by a mercury intrusion method. Further details can be found elsewhere.[33]

Dense 8YSZ tapes of 150-µm thickness were obtained from Kerafol, Germany. The tape was used as purchased to perform the microstructural analysis and the electrical conductivity measurements.

Microstructures: Top-view micrographs of the thin films were acquired by a scanning electron microscope (FEG-SEM, Zeiss LEO Gemini 1530,

Germany) with an in-lens detector. Prior to imaging, the thin films were coated with platinum in order to avoid charging and to allow imaging at higher resolutions.

Scanning transmission electron microscopy (STEM) in high-angle annular dark-field (HAADF) mode was used to characterize the microstructure of the thin films on sapphire. The microscope was a FEI Tecnai F-30 (field emission gun) with an accelerating voltage of 300 kV and post-column CCD camera. Cross-sectional TEM lamellae of thin films deposited on silicon substrates were prepared traditionally by polishing, dimpling and ion milling (Gatan precision ion polishing system at 3.5 keV and 4.0 ° angle of incidence from top and bottom). TEM lamellae for the cross-sectional views of the thin films deposited on sapphire substrates were prepared by focused ion beam (FIB) technique on a CrossBeam NVision 40 from Carl Zeiss with a gallium liquid metal ion source, a gas injection system and a micromanipulator MM3A from Kleindiek. After electron beam deposition of carbon in SEM mode at low scan rate, thin films were protected by a carbon cap. TEM lamellae were cut free with trenches from both sides with 13 and 3 nA at 30 kV. After the lift-out was performed, the lamellae were polished to ion transparency with currents down to 10 pA at 30 kV. The amorphization was diminished by low kV showering for several seconds at 5 and 2 kV.

Electrical Characterization: For the electrical characterization, YSZ thin films were deposited on randomly-oriented sapphire single crystals (Stettler, Switzerland) which were coated with approximately 10 nm sputtered tantalum (as adhesion layer) and 100 nm platinum (as bottom electrode). On the thin films, platinum electrodes (as top electrode) with different sizes in the range of 0.2 to 9 mm^2 were sputtered. The standard size was 1 mm^2. The electrodes were contacted by microprobes and the samples were measured on a hot-plate in ambient air. The temperature was measured with a thermocouple placed on sapphire right next to the sample. For measurements as a function of humidity, synthetic air (150 sccm) was passed through a bubbler with water at 50 °C and directed to the sample using a funnel.

Porous 3YSZ samples and dense 8YSZ tape were contacted on both sides with platinum sputtered through a shadow mask, platinum paste (C 3605 S, Heraeus, Germany) and platinum wire. The temperature of the sample was measured with a thermocouple placed right next to the sample in the heating furnace. The air flow in the furnace of 50 sccm was dried over silica gel or moistened through a water bubbler heated at 25 or 60 °C.

Electrical impedance was measured by an impedance bridge (Zahner IM6, Zahner Electric, Germany; and Solatron 1260, Solartron Analytical, UK), operated between 100 mHz and 4 MHz using an oscillation amplitude of 20 mV. The impedance spectra were recorded during heating and cooling at a rate of 1 °C min^{-1}. The conductivity of porous 3YSZ pellet and the dense 8YSZ tape were measured in direct current pseudo 4-probe mode in air. The resistance was measured during heating and cooling at a rate of 3 °C min^{-1} by a multimeter (Keithley 2700) and recorded every 30 s by a custom made LabView program. From the resistance (R) of the electrolyte contribution, the electrode area, film thickness, and the total conductivity of the specimens were obtained. The porosity was not considered in the calculation.

Acknowledgements

B.S., M.S., D.S., J.G., H.M. and P.K. prepared the specimens. B.S., M.S., D.S., J.M., J.G. and H.M. performed the experiments with the technical help and advice of B.S., M.S., J.M., T.L., M.P. and L.G.; B.S. wrote the manuscript in collaboration with all the other co-authors. The authors thank Thomas Ryll, Henning Galinski, Pascal Wettstein, Anna Evans, Samuel Zimmermann and Frank Filser for stimulating discussions. The authors acknowledge support by the Electron Microscopy of ETH Zurich (EMEZ). Financial support by the Swiss National Foundation (SNF) within the framework of the Sinergia project CRSI22-126830 and the Korean-Swiss Science and Technology Cooperation is gratefully acknowledged. L.J.G. gratefully acknowledges the support of the International Institute for Carbon Neutral Energy Research (WPI-I^2CNER), sponsored by the World Premier International Research Center Initiative (WPI), MEXT, Japan.

Received: July 18, 2012
Published online: November 15, 2012

[1] a) H. Huang, M. Nakamura, P. C. Su, R. Fasching, Y. Saito, F. B. Prinz, *J. Electrochem. Soc.* **2007**, *154*, B20; b) U. P. Muecke, D. Beckel, A. Bernard, A. Bieberle-Hütter, S. Graf, A. Infortuna, P. Müller, J. L. M. Rupp, J. Schneider, L. J. Gauckler, *Adv. Funct. Mater.* **2008**, *18*, 3158; c) A. Evans, A. Bieberle-Hütter, J. L. M. Rupp, L. J. Gauckler, *J. Power Sources* **2009**, *194*, 119; d) S. Rey-Mermet, Y. Yan, C. Sandu, G. Deng, P. Muralt, *Thin Solid Films* **2010**, *518*, 4743; e) I. Garbayo, A. Tarancón, J. Santiso, F. Peiró, E. Alarcón-Lladó, A. Cavallaro, I. Gràcia, C. Cané, N. Sabaté, *Solid State Ionics* **2010**, *181*, 322; f) C.-W. Kwon, J.-W. Son, J.-H. Lee, H.-M. Kim, H.-W. Lee, K.-B. Kim, *Adv. Funct. Mater.* **2011**, *21*, 1154; g) M. Tsuchiya, B.-K. Lai, S. Ramanathan, *Nat. Nano* **2011**, *6*, 282; h) B.-K. Lai, K. Kerman, S. Ramanathan, *J. Power Sources* **2011**, *196*, 1826; i) K. Kerman, B.-K. Lai, S. Ramanathan, *J. Power Sources* **2011**, *196*, 2608.

[2] a) C. Wagner, *Ber. Bunsen Ges.* **1968**, *72*, 778; b) Y. Nigara, K. Yashiro, J. O. Hong, T. Kawada, J. Mizusaki, *Solid State Ionics* **2004**, *171*, 61.

[3] Y. Nigara, K. Yashiro, T. Kawada, J. Mizusaki, *Solid State Ionics* **2003**, *159*, 135.

[4] M. Shirpour, G. Gregori, R. Merkle, J. Maier, *Phys. Chem. Chem. Phys.* **2011**, *13*, 937.

[5] H. J. Avila-Paredes, E. Barrera-Calva, H. U. Anderson, R. A. De Souza, M. Martin, Z. A. Munir, S. Kim, *J. Mater. Chem.* **2010**, *20*, 6235.

[6] a) H. J. Avila-Paredes, J. Zhao, S. Wang, M. Pietrowski, R. A. De Souza, A. Reinholdt, Z. A. Munir, M. Martin, S. Kim, *J. Mater. Chem.* **2010**, *20*, 990; b) G. Chiodelli, F. Maglia, U. Anselmi-Tamburini, Z. A. Munir, *Solid State Ionics* **2009**, *180*, 297; c) S. Kim, H. J. Avila-Paredes, S. Wang, C.-T. Chen, R. A. De Souza, M. Martin, Z. A. Munir, *Phys. Chem. Chem. Phys.* **2009**, *11*, 3035; d) E. Ruiz-Trejo, J. Kilner, *J. Appl. Electrochem.* **2009**, *39*, 523.

[7] H. J. Avila-Paredes, C.-T. Chen, S. Wang, R. A. De Souza, M. Martin, Z. Munir, S. Kim, *J. Mater. Chem.* **2010**, *20*, 10110.

[8] H. Takamura, N. Takahashi, *Solid State Ionics* **2010**, *181*, 100.

[9] C. Tande, D. Perez-Coll, G. C. Mather, *J. Mater. Chem.* **2012**, *22*, 11208.

[10] I. Riess, S. Raz, K. Sasaki, J. Maier, in *Ionic and Mixed Conducting Ceramics IV*(Ed: T. A. Ramanarayanan), Electroceramics Society, Pennington, New Jersey, USA **2002**, p. 267.

[11] S. Raz, K. Sasaki, J. Maier, I. Riess, *Solid State Ionics* **2001**, *143*, 181.

[12] J. Wang, M.-Y. Su, J.-Q. Qi, L.-Q. Chang, *Sens. Actuators, B* **2009**, *139*, 418.

[13] S. Kim, U. Anselmi-Tamburini, H. J. Park, M. Martin, Z. A. Munir, *Adv. Mater.* **2008**, *20*, 556.

[14] B. Scherrer, J. Martynczuk, H. Galinski, J. G. Grolig, S. Binder, A. Bieberle-Hütter, J. L. M. Rupp, M. Prestat, L. J. Gauckler, *Adv. Funct. Mater.* **2012**, *22*, 3509.

[15] B. Scherrer, S. Heiroth, R. Hafner, J. Martynczuk, A. Bieberle-Hütter, J. L. M. Rupp, L. J. Gauckler, *Adv. Funct. Mater.* **2011**, *21*, 3967.

[16] M. V. F. Schlupp, M. Prestat, J. Martynczuk, J. L. M. Rupp, A. Bieberle-Hütter, L. J. Gauckler, *J. Power Sources* **2012**, *202*, 47.

[17] M. V. F. Schlupp, J. Martynczuk, M. Prestat, L. J. Gauckler, *Adv. Eng. Mater.* **2012** DOI:10.1002/aenm.201200596.

[18] S. Heiroth, T. Lippert, A. Wokaun, M. Dobeli, J. L. M. Rupp, B. Scherrer, L. J. Gauckler, *J. Eur. Ceram. Soc.* **2010**, *30*, 489.

[19] A. Infortuna, A. S. Harvey, L. J. Gauckler, *Adv. Funct. Mater.* **2008**, *18*, 127.

[20] M. V. F. Schlupp, B. Scherrer, H. Ma, J. G. Grolig, J. Martynczuk, M. Prestat, L. J. Gauckler, *Phys. Status Solidi A* **2012**, *209*, 1414.
[21] X. Guo, E. Vasco, S. Mi, K. Szot, E. Wachsman, R. Waser, *Acta Mater.* **2005**, *53*, 5161.
[22] a) M. Fronzi, S. Piccinin, B. Delley, E. Traversa, C. Stampfl, *Phys. Chem. Chem. Phys.* **2009**, *11*, 9188; b) A. Kossoy, H. Cohen, T. Bendikov, E. Wachtel, I. Lubomirsky, *Solid State Ionics* **2011**, *194*, 1.
[23] S. Miyoshi, Y. Akao, N. Kuwata, J. Kawamura, Y. Oyama, T. Yagi, S. Yamaguchi, *Solid State Ionics* **2012**, *207*, 21.
[24] N. Yamazoe, J. Fuchigami, M. Kishikawa, T. Seiyama, *Surf. Sci.* **1979**, *86*, 335.
[25] H. A. Al-Abadleh, V. H. Grassian, *Surf. Sci. Rep.* **2003**, *52*, 63.
[26] a) S. Hara, S. Takano, M. Miyayama, *J. Phys. Chem. B* **2004**, *108*, 5634; b) W. A. England, M. G. Cross, A. Hamnett, P. J. Wiseman, J. B. Goodenough, *Solid State Ionics* **1980**, *1*, 231.
[27] a) K. D. Kreuer, *Solid State Ionics* **1997**, *94*, 55; b) I. Alkorta, J. Elguero, *Org. Biomol. Chem.* **2006**, *4*, 3096.
[28] a) F. M. Vichi, M. T. Colomer, M. A. Anderson, *Electrochem. Solid-State Lett.* **1999**, *2*, 313; b) M. I. Tejedor-Tejedor, F. M. Vichi, M. A. Anderson, *J. Porous Mater.* **2005**, *12*, 201; c) Y. Ben-Da, S. Meilink, G. Warren, P. Wynblatt, *IEEE Trans. Components, Hybrids, and Manufacturing Technology* **1987**, *10*, 247; d) M. T. Colomer, *J. Eur. Ceram. Soc.* **2006**, *26*, 1231.
[29] G. Ketteler, S. Yamamoto, H. Bluhm, K. Andersson, D. E. Starr, D. F. Ogletree, H. Ogasawara, A. Nilsson, M. Salmeron, *J. Phys. Chem. C* **2007**, *111*, 8278.
[30] a) N. Rana, P. Raghu, E. Shero, F. Shadman, *Appl. Surf. Sci.* **2003**, *205*, 160; b) P. Raghu, C. Yim, F. Shadman, E. Shero, *AIChE J.* **2004**, *50*, 1881.
[31] a) O. Wilhelm, S. E. Pratsinis, D. Perednis, L. J. Gauckler, *Thin Solid Films* **2005**, *479*, 121; b) D. Perednis, O. Wilhelm, S. E. Pratsinis, L. J. Gauckler, *Thin Solid Films* **2005**, *474*, 84.
[32] B. Scherrer, A. Rossi, J. Martynczuk, M. D. Rossell, A. Bieberle-Hütter, J. L. M. Rupp, R. Erni, L. J. Gauckler, *J. Power Sources* **2011**, *196*, 7372.
[33] a) F. Filser, PhD Thesis, Swiss Federal Institute of Technology, Zurich **2001**; b) F. Filser, P. Kocher, F. Weibel, H. Lüthy, P. Schärer, L. J. Gauckler, *Int. J. Comp. Dent.* **2001**, *4*, 89.